A

allele	$dNrd1^A$	$dNrd1^B$	$dNrd1^C$	$dNrd1^D$
$dNrd1^A$	pupa			
$dNrd1^B$	pupa	pupa		
$dNrd1^C$	pupa	pupa	pupa	
$dNrd1^D$	pupa	pupa	pupa	pupa

B

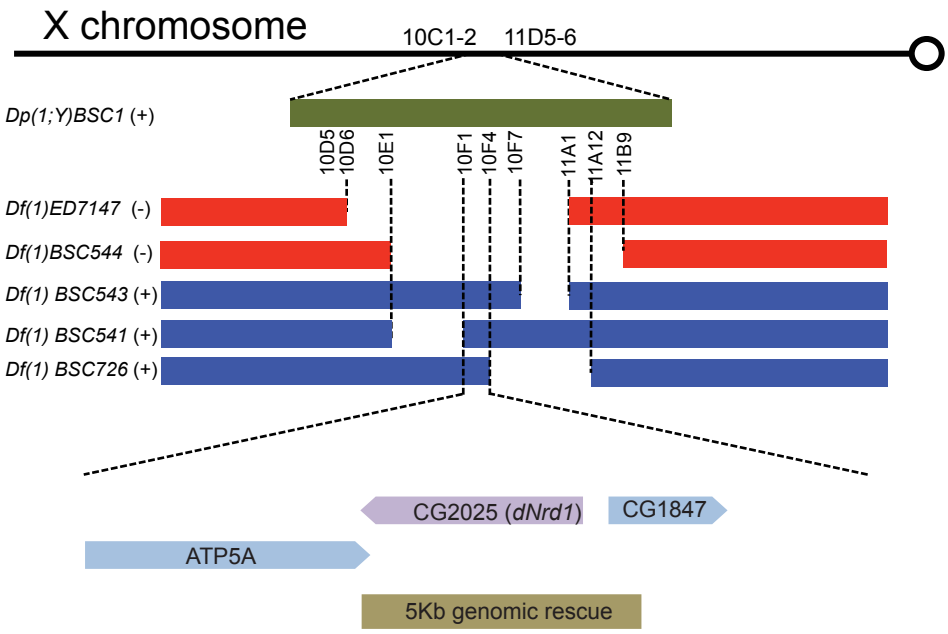

C

transgene \ allele	$dNrd1^A$	$dNrd1^B$	$dNrd1^C$	$dNrd1^D$
80kb P[acman] Dp(1;3)DC246	+	+	+	+
20kb P[acman] CH322-77E05	+	+	+	+
5kb genomic rescue	+	+	+	+
Ubiquitous-Gal4 >UAS-dNrd1-V5	+	+	+	+
Ubiquitous-Gal4> UAS-human NRD1-V5	+	+	+	+
Ubiquitous-Gal4> UAS-human NRD1 (M636Vstop)-V5	-	-	-	-
Ubiquitous-Gal4 >UAS-dNrd1-mcherry	-	-	-	-

D

Species		*H. sapiens*	*B. taurus*	*M. musculus*	*R. norvegicus*	*G. gallus*
DNRD1	Identity	37%	37%	37%	37%	36%
	Similarity	58%	58%	58%	58%	58%

Figure S1

A

S2 cells

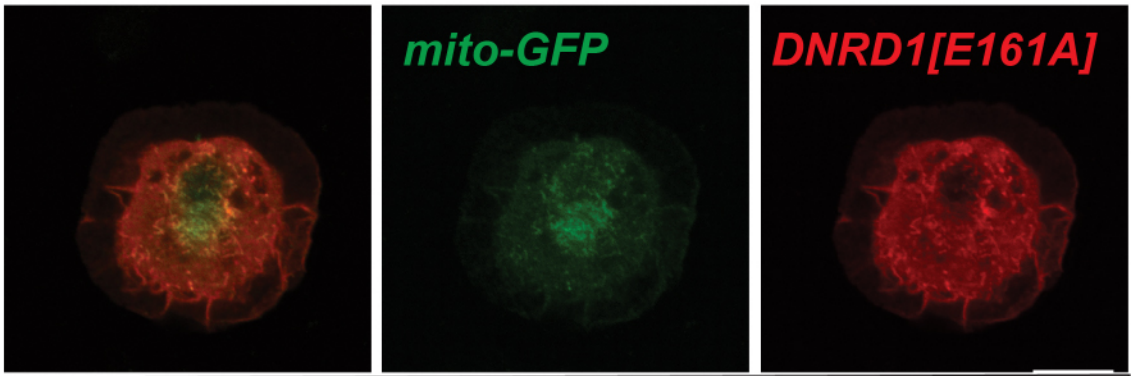

Act-Gal4>UAS-dNrd1 [E161A]

B

Muscle

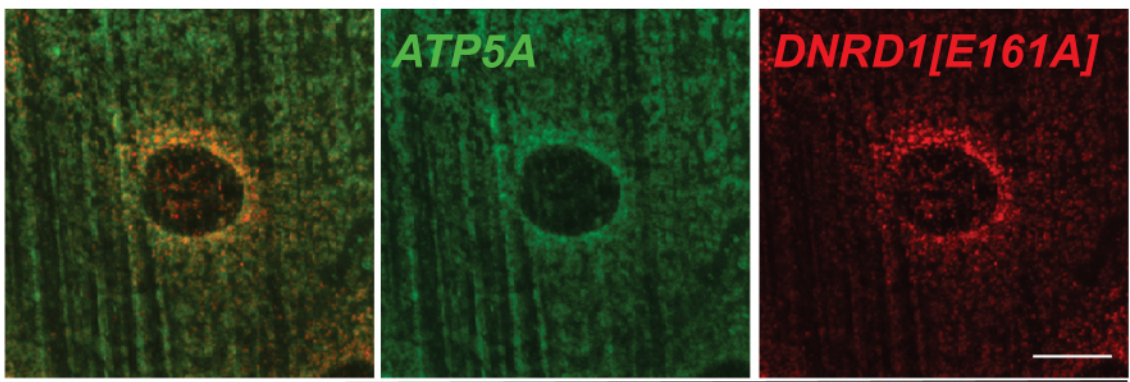

C57-Gal4>UAS-dNrd1 [E161A]

dNrd1^{c}/y

Figure S2

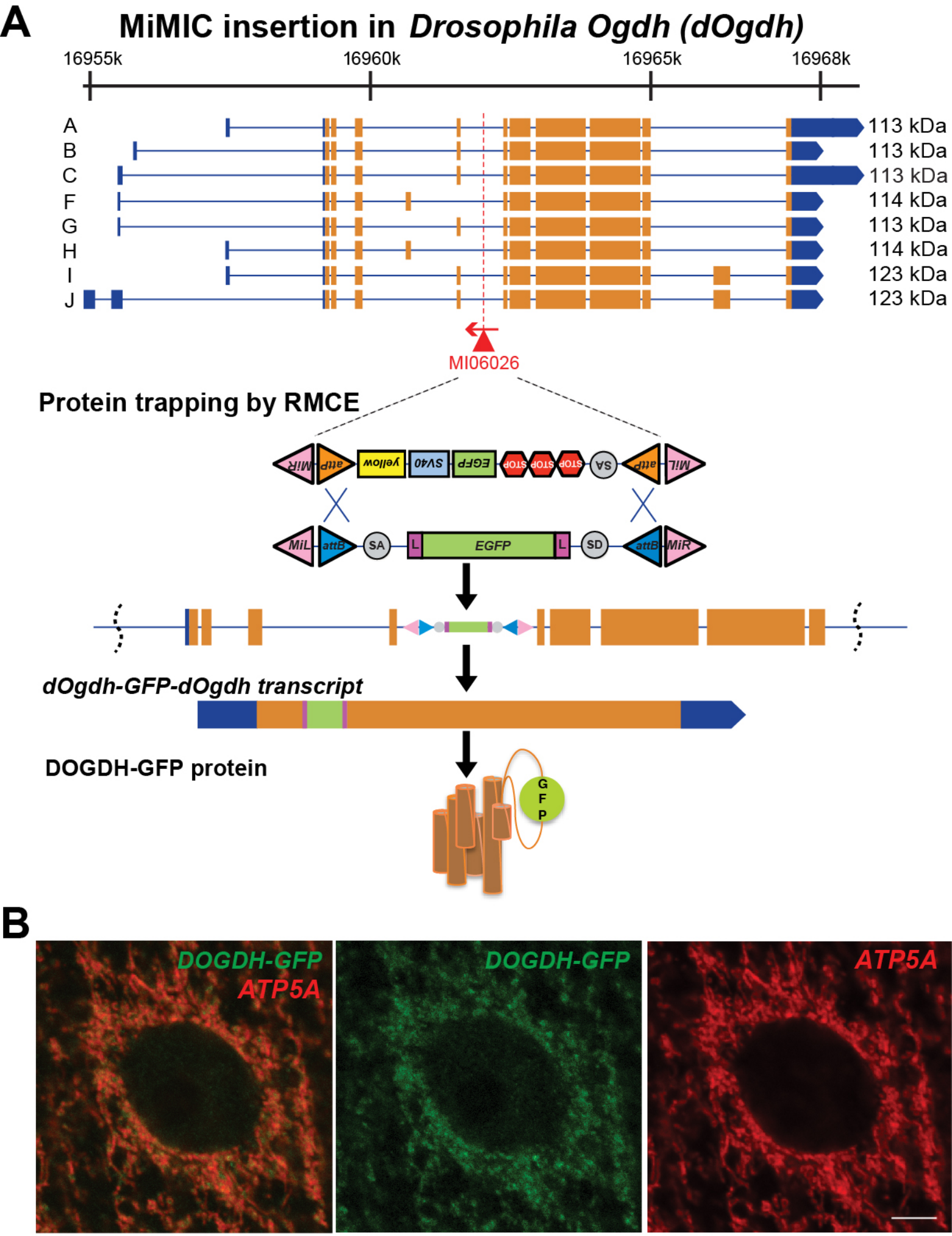
A
MiMIC insertion in Drosophila Ogdh (dOgdh)
16955k
16960k
16965k
16968k
A
B
C
F
G
H
I
J
113 kDa
113 kDa
113 kDa
114 kDa
113 kDa
114 kDa
123 kDa
123 kDa
MI06026
Protein trapping by RMCE
MiL
attB
SA
L
EGFP
L
SD
attB
MiR
dOgdh-GFP-dOgdh transcript
DOGDH-GFP protein
G
F
P
B
DOGDH-GFP
ATP5A
DOGDH-GFP
ATP5A

Figure S3

A

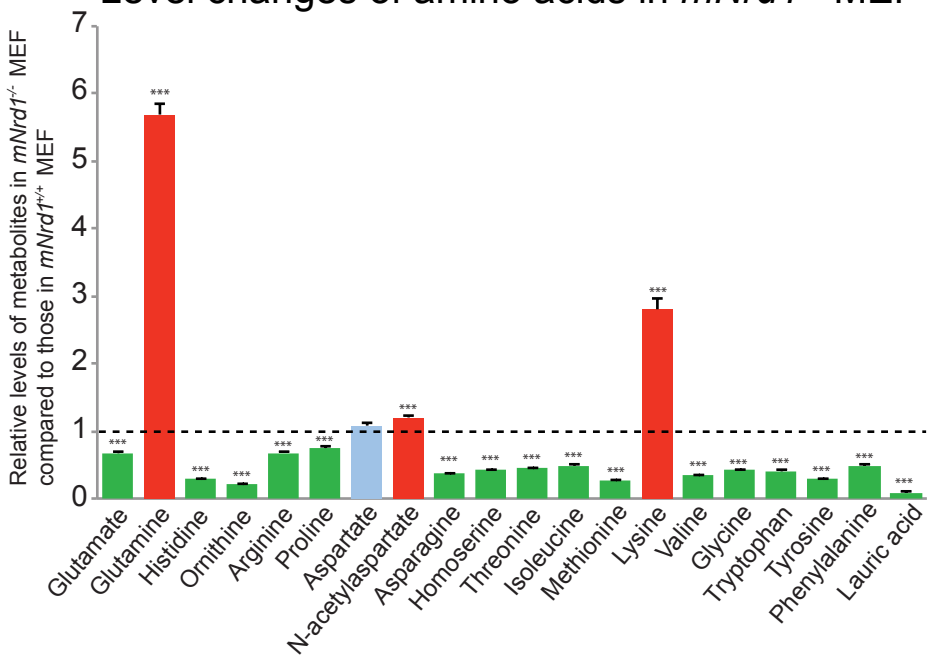

B

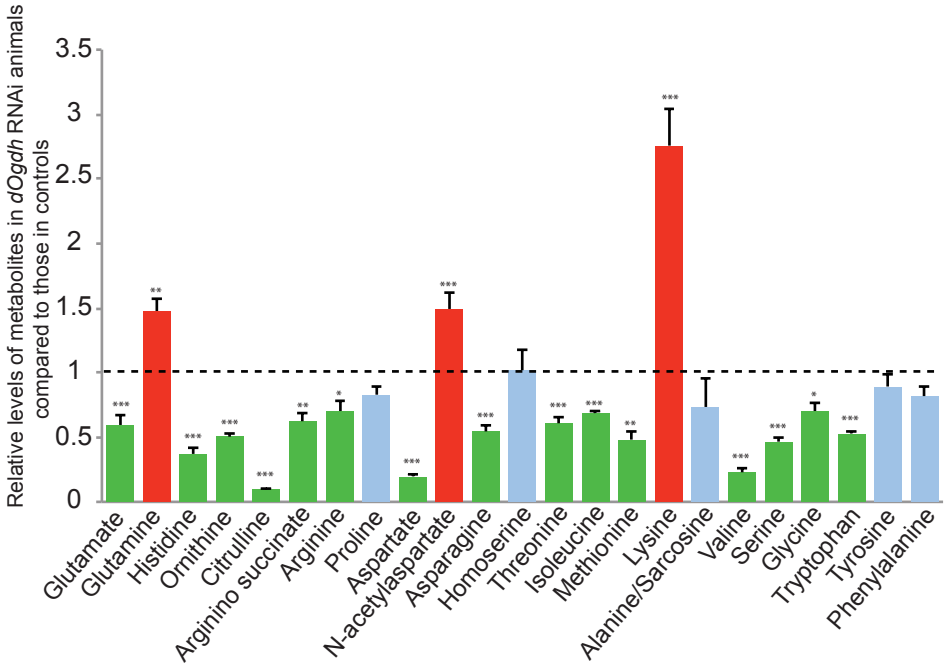

C

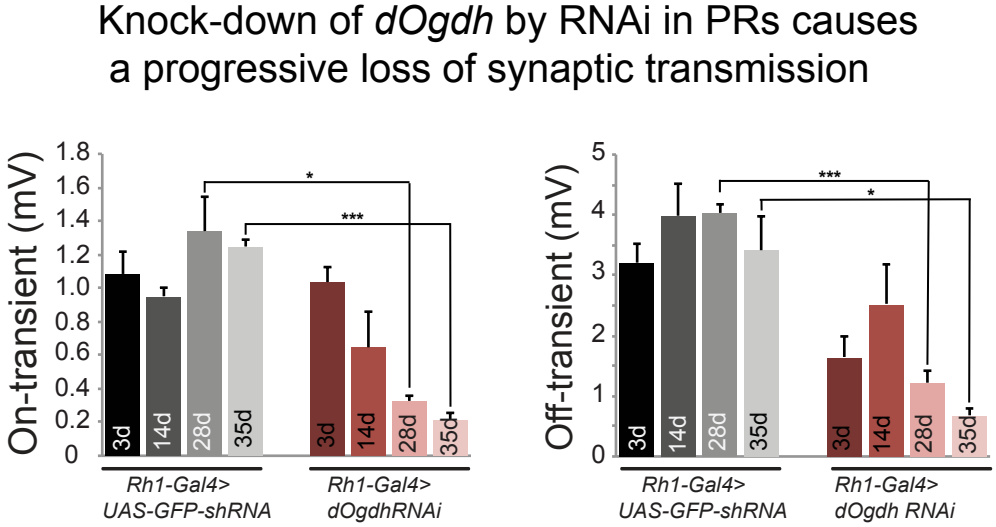

Figure S4

A

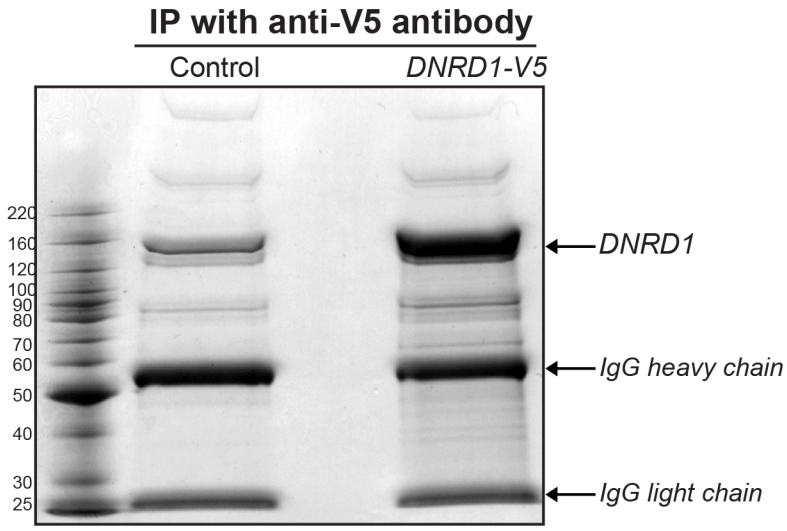

B

Subcomplexes of NRD1-interacting mitochondrial proteins

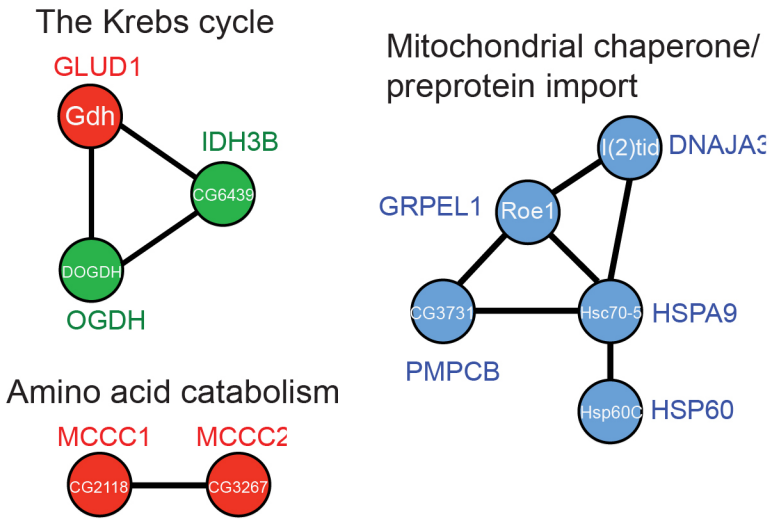

C

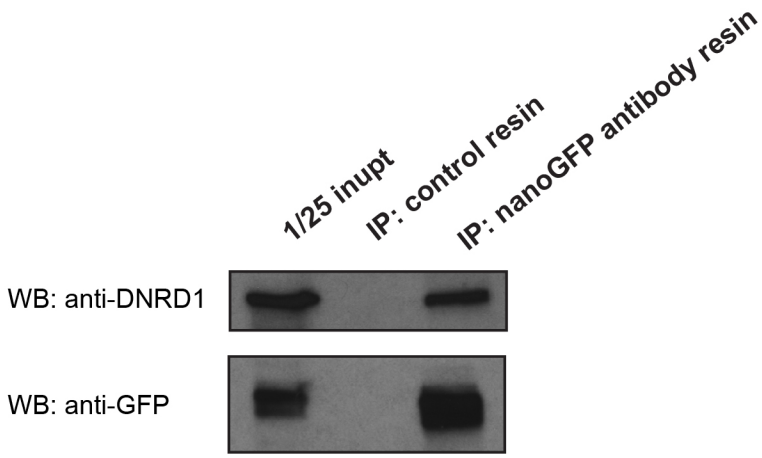

Figure S5

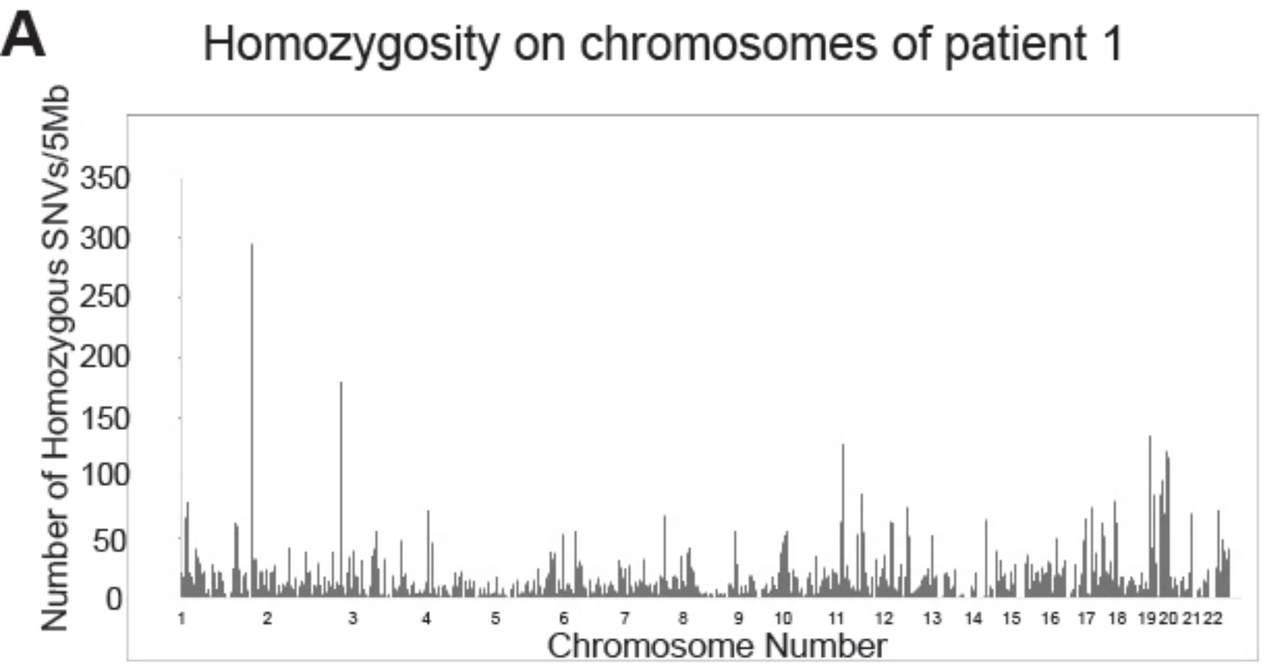
A
Homozygosity on chromosomes of patient 1
Number of Homozygous SNVs/5Mb
Chromosome Number
B
Head circumference of patient 1
Head circumference (cm)
Age (months)
C
Head circumference of patient 1 and 2
Head circumference (CM)
+ 2 SD (98%)
mean (50%)
- 2 SD (2%)
Patient 1 with NRD1 variant
Patient 2 with OGDHL variant
Age (years)
D
A T2 midaxial image of patient 2 at age 15 years
E
Absence of heterozygosity on chromosome 10 in patent 2
Variences/total reads ratio
Chromosome 10
OGDHL
F
Clinical photograph of patient 2
G
Lateral ventricle
3rd ventricle
Age 6
Age 14
H
Expression of wildtype OGDHL and OGDH, not mutants rescues ERG defects caused by knockdown of dOgdh
On-transient (mV)
Off-transient (mV)
Rh1-Gal4
Rh-Gal4
dOgdh RNAi
dOgdh
dOgdh(S793L)
OGDHL
OGDHL(S778L)
OGDH
OGDH(S791L)

Figure S6

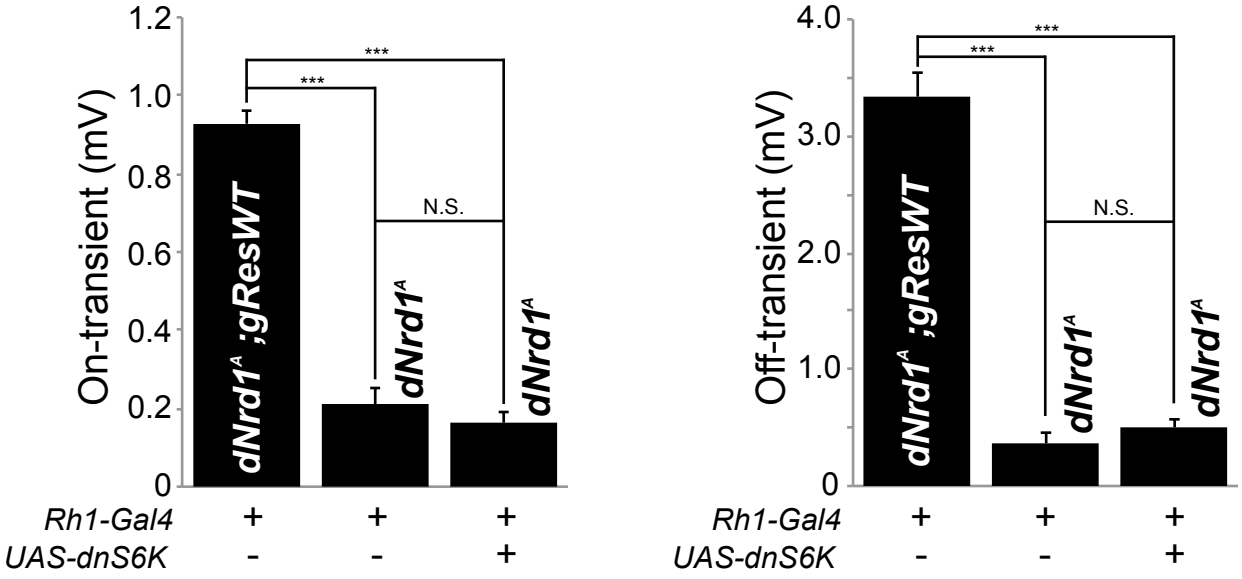
On-transient (mV)
1.2
1.0
0.8
0.6
0.4
0.2
0
***
***
N.S.
dNrd1A;gResWT
dNrd1A
dNrd1A
Rh1-Gal4 + + +
UAS-dnS6K - - +
Off-transient (mV)
4.0
3.0
2.0
1.0
0
***
***
N.S.
dNrd1A;gResWT
dNrd1A
dNrd1A
Rh1-Gal4 + + +
UAS-dnS6K - - +

Figure S7

Supplemental Figure Legends

Figure S1 (Related to Figure 1). Mapping, lethal staging, lethality rescue and evolutionary conservation of *dNrd1*

(A) Lethal staging analysis of four *dNrd1* mutant alleles. (B) Schematic representation of the *dNrd1* locus on the *Drosophila* X chromosome. The dark green bar indicates a large duplication that complements the lethality of mutants. Red bars indicate deficiencies that fail to complement the lethality of mutants. Blue bars indicate deficiencies that complement the lethality of the mutants. (+) indicates complementation. (-) indicates failure of complementation. A 5kb genomic rescue fragment encompassing the *dNrd1* locus (olive green) was used for most assays. (C) The lethality of *dNrd1* mutants was rescued by 80kb *P[acman]* genomic transgene, 20kb *P[acman]* genomic transgenes, 5kb genomic transgene carrying *dNrd1* genomic locus, expressing C-terminally V5 tagged *dNrd1* cDNA ubiquitously (*da-GAL4>UAS- dNrd1-V5*), or expressing C-terminally V5 tagged human *NRD1* cDNA ubiquitously (*da-GAL4>UAS- NRD1-V5*). Expression of the truncated human *NRD1* (p.M636VfsX2) variant identified from patient 1 did not rescue the lethality associated with *dNrd1* mutants, indicating that the p.M636VfsX2 variant is indeed a strong loss of function allele. Rescue was not achieved by expressing a C-terminally mCherry tagged *dNrd1* ubiquitously (*da-GAL4>UAS- dNrd1-mCherry*), indicating that the mCherry tagged DNRD1 is not functional. Overexpression of *dNrd1-mCherry* ubiquitously in a wild-type background kills the animals (data not shown), suggesting that DNRD1-mCherry acts as a dominant negative protein. We also found that this protein does not localize to the mitochondria, so *UAS-dNrd1-mCherry* transgenic flies was not further used in the following studies (D) The amino acid sequences of NRD1 are conserved from fruit fly to mammals.

Figure S2 (Related to Figure 2). Point mutation [E161A] in DNRD1 alters subcellular localization of DNRD1

(A) Confocal micrographs of S2 cells co-expressing mito-GFP (green) and *dNrd1* carrying point mutation (E161A) (*dNrd1[E161A]-V5*), (red). Scale bars, 10μm. (B) Confocal micrographs of $dNrd1^{C}$ mutant larval muscle expressing *dNrd1[E161A]-V5* (red) by muscle driver (*C57-Gal4*). ATP5A (green) labels mitochondria. Scale bars, 10μm.

Figure S3 (Related to Figure 4). Generation of intronic GFP-tagged *dOgdh*

(A) MiMIC insertion in *dOgdh* (also referred to as *Neural conserved at 73EF* (*Nc73EF*): [Top] A schematic of the *dOgdh* gene region based on FlyBase annotation release FP2014_06. The orange boxes indicate coding exons. Dark blue boxes indicate 5'- and 3'-UTR. The isoforms are labeled by the names and molecular weights of the translated proteins. The Mi{MIC} insertion, *MI06026* is indicated by the red triangle and its insertion position is shown by a red dotted line. [Middle] Protein trapping by Recombinase-Mediated Cassette Exchange (RMCE): The MiMIC transposable element consists of a splice acceptor (SA; gray) followed by stop codons in all three reading frames (red), an EGFP coding sequence (green), a SV40 polyadenylation signal (pale blue), and the $yellow^{+}$ marker (yellow). Two inverted *attP* sites (orange) and two *Minos* inverted repeats (pink) are positioned at the 5'- and 3'-end of the transposon. The protein trap cassette consists of a SA (gray), an EGFP coding sequence (green) flanked by linker sequences (purple) and a splice donor (SD; gray). [Bottom] When transcribed and translated, DOGDH is internally tagged with EGFP. (B) Confocal micrographs of larval muscle in a fly carrying an artificial exon that encodes EGFP, inserted in a coding intron of *dOgdh*. The EGFP-tagged DOGDH protein (DOGDH-GFP) is detected by anti-GFP antibody (green). ATP5A (red) labels mitochondria. Scale bars, 5μm.

Figure S4 (Related to Figure 4). Knockdown of *dOgdh* phenocopies loss of *Nrd1* in fly and *mNrd1* in MEF

(A) LC-MS analysis of ratio of amino acids levels of $mNrd1^{-/-}$ MEF to those in wild type MEF. (B) LC-MS analysis of ratio of amino acids levels of *dOgdh RNAi* larvae (*UAS-dOgdh RNAi* (*v50393)/Actin-Gal4*) to those in control larvae (*+/Actin-Gal4*). Error bars indicate s.e.m. P values were calculated using Student's t-test. $*P < 0.05$, $**P < 0.01$, $***P < 0.001$. (C) Quantification of the on- and off-transients of ERGs in PRs where *dOgdh* is knockdowned

by RNAi (*Rh1-Gal4/UAS-dOgdh RNAi*) and control PRs (*Rh-1-Gal4>UAS-GFP-shRNA*) in flies aged for multiple time points. P values were calculated using Student's t-test. *P <0.05, ***P <0.001.

Figure S5 (Related to Figure 5). DNRD1 physically interacts with DOGDH as well as mitochondrial chaperones

(A) Anti-V5 antibody is used for immunoprecipitation. Arrows indicate enriched DNRD1 in immunoprecipitated proteins from C-terminally V5 tagged-DNRD1-expressing larvae (*da-Gal4>UAS-dNrd1-V5*), when compared to proteins immunoprecipitated from control larvae (*da-Gal4*, no *UAS*). The two other arrows indicate an IgG heavy chain and an IgG light chain, respectively. Numbers beside the molecular weight marker (the first lane) denote molecular weights. (B) Bioinformatics analyses based on STRING and COMPLEAT show three subcomplexes of DNRD1-interacting proteins. (C) Co-immunoprecipitation using anti-GFP nano-antibody from lysates of DOGDH-GFP larvae. Western blots were performed using either anti-DNRD1 or anti-GFP antibody.

Figure S6 (Related to Figure 6). Patients with *NRD1* or *OGDHL* variants exhibit neurodegenerative phenotypes

(A) A plot of the number of homozygous SNVs/5Mb on all chromosomes of the patient 1. (B) A graph of head circumference from birth to 26 months for patient 1. (C) A graph of head circumference of patient 1 (red circles) from age 5 to 14 and patient 2 from age 11 to 15 (blue circles). The solid line indicates the mean value of head circumference while upper and lower dotted lines indicate 98th and 2nd percentiles of head circumference, respectively. (D) A T2 midaxial image of patient 1 at age 15 years shows enlarged extracerebral spaces (red arrows). (E) A plot of the variant reads/ total reads ratio on chromosome 10 (i.e. B-allele frequency from WES data) with the grey shaded segments representing detected absence of heterozygosity (AOH) regions in the patient 2. Two blocks of AOH (gray vertical boxes) a large 5.101Mb and 1.287 Mb (chr10: 49,938,185-51,225,724) are observed on chromosome 10. The smaller interval encompasses the position of the *OGDHL* gene (GRCH27/hg19, chr10:50,942,687-50,970,425; red vertical line) in which the homozygous variants were observed. (F) Clinical photograph of patient 2 (Individual BAB4852). (G) Comparison of cerebral MRI images of patient 2 at age 6 and 14. Note the enlargement of temporal horns of the lateral ventricle and 3rd ventricle (yellow crossmarks). (H) Quantification of the on- and off-transients of ERGs in PRs expressing *dOgdh RNAi* (*Rh1-Gal4/UAS-dOgdh RNAi*), together with *UAS* only (2nd bar of each graph), *UAS-dOgdh*, *UAS-dOgdh^{S793L}*, *UAS-human OGDHL*, *UAS-human OGDHL^{S778L}*, *UAS-human OGDH*, or *UAS-human OGDH^{S791L}* in 21-day-old flies. Expression of human OGDH^{WT} or OGDHL^{WT} rescues the ERG defects caused by knockdown of *dOgdh*, but expression of human OGDH^{S791L} or OGDHL^{S778L} fails to rescue. Error bars indicate s.e.m. P values were calculated using Student's t-test. *P <0.05, **P <0.01, ***P <0.001.

Figure S7 (Related to Figure 7). Expression of dominant negative S6K fails to rescue the ERG defects in *dNrd1* mutants

Quantification of the on- and off-transients of ERGs in 35-day-old *dNrd1^{A}* mutant clones in PRs with or without expressing *dominant negative S6K* (*Rh1-Gal4>UAS-S6k.KQ*) and control PRs (*dNrd1^{A}; gRes-WT*). Error bars indicate s.e.m. P values were calculated using Student's t-test. ***P <0.001. N.S. indicates not statistically significant.

Supplemental Tables

Table S1: The list of DNRD1-interacting proteins, related to Figure 5

IP/MS from C-terminally V5 tagged DNRD1 identified DNRD-interacting proteins that include mitochondrial chaperone proteins (blue) as well as metabolic enzymes in the TCA cycle (green), Amino acid metabolism (red), glucose metabolism (orange), and lipid metabolism (yellow).

Table S2: The list of candidate variants in Patient 1 and Patient 2, related to Figure 6

WES on eight individuals in *NRD1* family identified homozygous variants and compound heterozygous variants unique in Patient 1. WES on parents and proband in *OGDHL* family identified homozygous variants, compound heterozygous variants, and *de novo* variants unique in Patient 2.

Table S3: Neurological Phenotypes of *Nrd1* knockout mice, Patient 1 and Patient 2, related to Figure 6 and discussion

Similarities and differences of neurological phenotypes among *Nrd1*$^{-/-}$ mouse, Patient 1 with homozygous recessive *NRD1* variant (NM_002525.2:exon 17:c.1906_1907delAT: p.M636VfsX2)] and Patient 2 with homozygous recessive *OGDHL* variant (NM_018245:exon18:c.C2333T:p.S778L).

Supplemental Table 1

Fly ID no.	Fold enrichemnt in DNRD1 Sample	*Drosophila*	Human homologue	mitochondrial protein	pathway
FBgn0030344	1033	CG2025	NRD1		MPP
FBgn0001220	93	Hsc70-5	HSPA9	mitochondrial	mitochondrial chaperone
FBgn0003888	68	βTub60D			cytoskeleton
FBgn0000043	55	Act42A			cytoskeleton
FBgn0001128	53	Gpdh	GPD1		glycolysis
FBgn0000046	49	Act87E			cytoskeleton
FBgn0037607	47	CG8036	TKTL2		pentose phosphate pathway
FBgn0038681	43	Cyp12a4			
FBgn0001098	37	Gdh	GLUD1	mitochondrial	amino acid catabolism
FBgn0031728	35	Hsp60C	HSP60	mitochondrial	mitochondrial chaperone
FBgn0032069	32	CG9468			
FBgn0250906	24	Pgk (phosphog	PGK1		glycolysis
FBgn0036892	23	Lon	LONP1	mitochondrial	mitochondrial protease/chaperone
FBgn0030737	23	CG9914	CRYL1		glucose catablism
FBgn0004907	23	14-3-3ζ			
FBgn0010352	22	Nc73EF	OGDH	mitochondrial	the TCA cycle
FBgn0034087	21	clu		mitochondrial	mitochondria biogenesis
FBgn0039877	20	CG2118	MCCC1	mitochondrial	amino acid catabolism
FBgn0026761	20	Trap1	TRAP1	mitochondrial	mitochondrial chaperone
FBgn0023507	19	CG3835	D2HGDH	mitochondrial	amino acid catabolism
FBgn0031703	19	CG12512	ACSF2	mitochondrial	lipid metabolism
FBgn0016715	17	Reg-2		mitochondrial	
FBgn0038922	17	CG6439	IDH3B	mitochondrial	the TCA cycle
FBgn0020238	16	14-3-3ε	YWHAE		
FBgn0038680	16	Cyp12a5			
FBgn0040237	16	bor	ATAD3A	mitochondrial	nucleoids stabilization
FBgn0002174	15	l(2)tid	DNAJ3	mitochondrial	mitochondrial chaperone
FBgn0031908	15	CG5177			
FBgn0024556	14	EfTuM	TUFM	mitochondrial	translation in mitohcondria
FBgn0011661	14	Moesin	MSM		cytoskeleton
FBgn0026370	14	SRPK	SRPK1		splicing
FBgn0053196	13	dp			
FBgn0024958	13	Irp-1A	ACO1		the TCA cycle
FBgn0024238	13	Fimbrin	LCP1		cytoskeleton
FBgn0038271	13	CG3731	PMPCB	mitochondrial	mitochondrial processing peptidase
FBgn0063497	12	GstE3			redox

FBgn0032889	12	CG9331			
FBgn0004868	12	Gdi	GDI1		
FBgn0003942	11	RpS27A	RPS27A		
FBgn0037913	11	fabp	FABP7		
FBgn0086347	11	Myo31DF	MYO1D		cytoskeleton
FBgn0051354	10	Hsp70Bbb	HSPA1A		chaperone
FBgn0261565	10	Lmpt	FHL2		
FBgn0029823	10	CG3011	SHMT1	mitochondrial	1-carbon metabilism-purine biosythesis
FBgn0034046	10	tun	WDYHV1		
FBgn0003189	10	r	CAD		pyrimidine biosynthesis
FBgn0026415	10	Idgf4			
FBgn0027590	10	GstE12			redox
FBgn0027779	10	VhaSFD	ATP6V1H		
FBgn0032715	10	CG17597			
FBgn0265137	10	Spn42Da	SERPINI1		
FBgn0013954	10	FK506-bp2			
FBgn0031418	9	CG3609	DHDL	mitochondrial	xenobiotics
FBgn0014877	9	Roe1	GRPEL1	mitochondrial	mitochondrial chaperone
FBgn0042083	9	CG3267	MCCC2	mitochondrial	amino acid catabolism
FBgn0012034	9	AcCoAS	ACSS2		lipid
FBgn0038745	9	CG4538	CLPX	mitochondrial	mitochondrial protease/chaperone
FBgn0030968	9	CG7322	DCXR		glucose catablism

Color codings for the major pathways

TCA cycle
Amino acid metabolism
Glucose metabolism
Lipid metabolism
mitochondrial chaperone

Supplemental Table 2

Gene name	key	Zygosity	Mutation_type_.Refseq.	ExAC (MAF)	nsdb__SIFT_score	nsdb__SIFT_prediction	nsdb__Polyphen2_score	nsdb__Polyphen2_prediction	OMIM	Comments
Homozygous variants unique in proband in NRD1 family										
NRD1	1:52277741_CAT>C	Hom	frameshift_deletion	1.65E-05	n/a	n/a	n/a	n/a	NA	
FAM151A	1:55080445_C>T	Hom	nonsynonymous_SNV	7.43E-05	0.4	Tolerated	0.117	benign	NA	No known disease association, variants predicted benign
RNF34	12:121855611_G>A	Hom	nonsynonymous_SNV	0.004531	0.4	Tolerated	0	benign	NA	No known disease association, variants predicted benign
MYO7B	2:128387261_G>A	Hom	nonsynonymous_SNV	0.009255	0.92	Tolerated	0.003	benign	NA	No known disease association, variants predicted benign
CHMP3	2:86790453_T>A	Hom	nonsynonymous_SNV	8.25E-06	0.51	Tolerated	0	benign	NA	No known disease association, variants predicted benign
FAM205B	9:34835361_C>T	Hom	ncRNA_exonic	0	0.01	Tolerated	0.083	benign	NA	No known disease association, variants predicted benign
SSX6	X:47972582_G>A	Hom	ncRNA_exonic	1.14E-05	0.64	Tolerated	0	benign	NA	No known disease association, variants predicted benign
Compound het variants unique in proband in NRD1 family										
OBSCN	1:228481897_A>C	Het	nonsynonymous_SNV	0.01282	0.39	Tolerated	0	benign	NA	
OBSCN	1:228496025_C>G	Het	nonsynonymous_SNV	0	0.33	Tolerated	0	benign	NA	
PUS1	12:132416633_C>T	Het	intronic	0.04258	0.02	Tolerated	0.942	probably damaging	Mitochondrial myopathy and sideroblastic anemia 1 [MIM:600462]'	Variants uncertain significance, phenotype not consistent
PUS1	12:132416813_G>A	Het	nonsynonymous_SNV	0.01618	0.19	Tolerated	0	benign	'Mitochondrial myopathy and sideroblastic anemia 1 [MIM:600462]'	Variants uncertain significance, phenotype not consistent

Gene name	key	Zygosity	Mutation_type_.Refseq.	ExAC (MAF)	nsdb__SIFT_score	nsdb__SIFT_prediction	nsdb__Polyphen2_score	nsdb__Polyphen2_prediction	OMIM	Comments
Homozygous variants unique in proband in OGDHL family										
OGDHL	10:50946295_G>A	Hom	nonsynonymous_SNV	8.26E-06	1	Damaging	0.997	probably damaging	NA	
KIAA1632	18:43496517_G>C	Hom	nonsynonymous_SNV	0	0.782555	Tolerated	0.426007	possibly damaging	NA	No known disease association, variants predicted benign
CCT8	21:30428834_T>G	Hom	nonsynonymous_SNV	1.7E-05	0.806454	Tolerated	0.496407	possibly damaging	NA	No known disease association, variants predicted benign
TIAM1	21:32624256_C>T	Hom	nonsynonymous_SNV	0	0.54	Tolerated	0.001	benign	NA	No known disease association, variants predicted benign
WASL	7:123329207_T>A	Hom	splicing	0	0	n/a	0	n/a	NA	
ARAP1	11:72437677_C>T	Hom	nonsynonymous_SNV	0.002808	0.75	Tolerated	0.822	possibly damaging	NA	No known disease association, variants predicted benign
ATP8B1	18:55315737_G>A	Hom	nonsynonymous_SNV	0.000139	1	Damaging	0.97	probably damaging	Cholestasis, benign recurrent intrahepatic' MIM:243300	Variants uncertain significance, phenotype not consistent
ARL13B	3:93769712_C>G	Hom	nonsynonymous_SNV	0.006489	1	Damaging	0.78	possibly damaging	Joubert syndrome 8 [MIM:612291]'	Variants uncertain significance, phenotype not consistent
Compound het variants unique in proband in OGDHL family										
AP2A2	11:984758_C>G	Het	splicing	4.14E-05	0	n/a	0	n/a	NA	
AP2A2	11:988619_A>G	Het	nonsynonymous_SNV	0.00209	0	n/a	0	n/a	NA	
LAMA2	6:129786384_A>G	Het	nonsynonymous_SNV	0.000232	0.75	Tolerated	0.648998	possibly damaging	Muscular dystrophy, congenital merosin-deficient [MIM:607855]'	Variants uncertain significance, phenotype not consistent
LAMA2	6:129601231_C>T	Het	nonsynonymous_SNV	0.005031	0.97	Damaging	0.627746	possibly damaging	Muscular dystrophy, congenital merosin-deficient [MIM:607855]'	Variants uncertain significance, phenotype not consistent
OBSCN	1:228456440_G>A	Het	nonsynonymous_SNV	0	0	n/a	0	n/a	NA	
OBSCN	1:228461966_C>T	Het	nonsynonymous_SNV	0.000059	0	n/a	0	n/a	NA	
VWA3A	16:22142902_G>A	Het	splicing	0	0	n/a	0	n/a	NA	
VWA3A	16:22157653_T>A	Het	nonsynonymous_SNV	0	0	n/a	0	n/a	NA	
De Novo variants unique in proband in OGDHL family										
PTCHD2	1:11575517_G>T	Het	nonsynonymous_SNV	0	1	Damaging	0.985	probably damaging	NA	Variants uncertain significance, uncharacterized gene

Supplemental Table 3

Phenotypic Comparison	*Nrd1*$^{-/-}$ Mouse (Ohno et al. 2009)	Patient CDMD1122 *NRD1* c.1906_1907delAT p.Met636ValfsX2	Patient BAB4852 *OGDHL* c.C2333T p.S778L
Developmental delay	+	+	+
Microcephaly	+	+	+
Ataxia	+	+	+
Motor impairment	+	+	+
Optic nerve hypoplasia	N/A	+	N/A
Hypotonia	N/A	+	+
Language problem	N/A	+	+
Seizures	+	+	-
MRI: White matter abnormality	N/A	Apparently normal MRI at 8 years	+
corpus callosum abnormaility	Myelination defects	Apparently normal MRI at 8 years	Hypoplasia of the corpus callosum
Age of Onset	Birth	During the 1 year of life	During the 1 year of life
Survival	neurological symptoms after P30 with progression P90-1 year 80% die in perinatal period	Alive at 15 years of age. Sibling with similar presentation died at the age of 16 month.	Alive at 15 years of age. Sibling with similar presentation died at the age of 28 years after being bedridden for many years.

NA: not analyzed

Supplemental Experimental Procedures

Clinical Case Histories

Patient 1 – M636VfsX2 in *NRD1*

Patient 1 (CDMD1122), the proband in Figure 2A, is a 15 year old male with severe global developmental delay and ataxia. Birth and prenatal history were unremarkable, and the patient initially presented in the first year of life with developmental delay and episodes of ocular deviation, suggestive of seizure activity. EEG (electroencephalogram) was normal. Biochemical studies revealed a slightly elevated C0 (free carinitine) and C4 (butyryl-isobutyryl carnitine) suggestive of short chain acyl-CoA dehydrogenase (SCAD) deficiency. Quantitative urine organic acid analysis showed increased citric acid and milder elevations in urine suberic, sebacic, octanoic, and ethylmalonic acid, consistent with mild SCAD deficiency. *ACADS* (*acyl-CoA dehydrogenase, C-2 to C-3 short chain*) gene sequencing did not identify any pathogenic variants, but showed homozygosity for a susceptibility variant c.625G>A (van Maldegem et al., 2010). Furthermore, the natural history of SCAD did not account for the severity of his developmental delay, therefore this finding was regarded as incidental and not diagnostic. Plasma amino acid profile was normal. At age 4 years, a second EEG was performed due to recurrent episodes during which he would go limp and be cyanotic for more than a minute. EEG results demonstrated areas of focal seizure activity and seizure medication was initiated. Follow up EEG at age 7 years demonstrated continued abnormalities including with generalized slowing of the cerebral activity. Brain MRI findings at age 8 years were as noted in the main text and ophthalmologic exam showed mild optic atrophy. After being seizure-free for more than 3 years, another EEG was performed that was normal and seizure medications were discontinued. At age 14 years of age, the patient remained at the developmental age of 1 year old without spoken language. On clinical exam microcephaly (<3rd percentile) was noted without significant dysmorphic features. Head size measurements beyond 5 years of age showed more variability (Figure S6C) (Baxter et al., 2009). However, the measurements collected in the last 10 years document significant microcephaly (Figure S6C). MRI images at 8-years of age show cortical and cerebellar volume loss and enlarged extracerebral spaces (Figure 6C). The latter phenotype is more severe at 15 years of age (Figure S6D). At present he has dysphagia, absent speech, hypotonia, and ataxia. There was also hypotonia, poor motor skills, and inability to walk independently. With assistance, he had a wide based gait with ataxic features. His developmental progression over time was nearly stagnant with rare incremental gains in skills without significant regression in milestones consistently noted. Patient remains on a liquid to pureed diet due to difficulty swallowing, nausea, and chronic constipation. Additional workup prior to clinical exome sequencing included a normal karyotype, and SNP chromosomal microarray studies consistent with segmental homozygosity on multiple chromosomes but without copy number gains or losses.

The p.M636VfsX2 variant is within a stretch of homozygosity spanning 10Mb on chromosome 1 (Figure S6A). Over the proband's entire genome, we observed five stretches of homozygosity that are larger than 5Mb, accounting for 1.8% of genome. This amount of homozygosity in the genome is consistent with a distant relationship between the parents as they both originate from a remote village in Central America.

Patient 2 - S778L in *OGDHL*

Patient 2 (BAB4852), the proband in Figure 7D, is a 15 year old girl (BAB4852) with a corpus callosum abnormality. The birth and prenatal history were unremarkable with no evidence of trauma. The patient was able to sit unsupported after 1 year, but never walked and has remained wheelchair dependent. This patient currently has severe intellectual disability and motor dysfunction of unknown cause which had been previously attributed to with cerebral palsy. Her clinical exam revealed hypertonicity and spasticity in the lower extremities with increased deep tendon reflexes. No seizures have been documented. Clinical examination did not suggest any prominent dysmorphic features, although some synophyrs and a large mouth were noted (Figure S6F). A brain MRI at age 6 years was most significant for a hypoplastic corpus callosum. Prominent cerebellar volume loss was also noted. At age 14 years a repeat brain MRI was obtained and notable findings included enlarged temporal horns of the lateral ventricle and 3rd ventricle compared to those at age 6 (Figure S6G). The proband had an elder brother who died at age 28 years. His parents described a very similar progressive neurological decline, although he died several years before the sequencing evaluation of the proband and no DNA sample was available for study. Brain MRIs from the 6 year old proband revealed a hypoplastic corpus callosum and prominent cerebellar volume loss (Figure 6G).

Moreover, MRI images at 14 years of age exhibit enlarged temporal horns of the lateral ventricle and 3rd ventricle when compared to those at 6 years of age (Figure S6G). Head circumference at age 14 was below the 2nd percentile (Figure S6C).

Additional workup prior to the exome sequencing through the Center for Mendelian Genomics (CMG) also included normal urine organic acids and normal plasma amino acids. The patient had exome sequencing as part of a study within the CMG of a cohort of Turkish patients with brain malformations. She was found to have a homozygous variant in *OGDHL* (NM_018245:exon18:c.C2333T:p.S778L) (Figure 6E). The p.S778L variant occurs in one heterozygote in the ExAC database (MAF=8.26 E-06), indicating that this variant is extremely rare. We performed WES on the proband, and both parents yielding a set of candidate variants in 13 genes, 3 of which are in known disease genes inconsistent with the phenotypes (Supplemental Table 2). The proband carries one coding *de novo* variant in an uncharacterized gene in addition to eight candidates with homozygous variants (Supplemental Table 2). Of these eight candidates, the variants in five genes were predicted to be benign whereas three are potentially damaging. The allele found in *ARL13B* (JBTS8) [MIM:612291] was found to have a high frequency in the population, and the patient MRI was not consistent with the known syndrome linked to that gene (Joubert syndrome 8). *ATP8B1* has been linked with a liver cholestasis, a phenotype not observed in our patient (Supplemental Table 2).

Functional Validation of a Missense Variant in OGDHL in Patient 2

Functional validation of the missense variant in *OGDHL* required the generation of a severe loss of function mutation in *dOgdh*, assessment of the phenotypes associated with loss of *dOgdh in vivo*, rescue of the phenotypes with the fly and human cDNAs, and testing the missense variant observed in the patient for its ability to rescue the phenotypes. Unfortunately, ubiquitous Gal4 drivers such as *Actin-*, *tubulin-*, and *daughterless-Gal4* driving the UAS-human OGDH caused lethality in flies. This prompted us to test a novel strategy by expressing the human OGDH in the same expression pattern of *dOgdh in vivo*. By combining recently developed technologies and resources (Diao et al., 2015; Gnerer et al., 2015), we were able to create *dOgdh* mutant flies (*dOgdh-T2A-Gal4*) in which the T2A-Gal4 cassette is inserted in a common coding intron of *dOgdh*. The *Gal4* insertion in *dOgdh* locus leads to severe loss of function of *dOgdh* since homozygous *dOgdh-T2A-Gal4* animals die before 1st instar larvae stage. We show that expression of the wild-type human *OGDH* cDNA or wild-type *dOgdh* cDNA by the Gal4 expressed under control of the endogenous *dOgdh* promoter (*dOgdh-T2A-Gal4*) rescued the lethality associated with loss of *dOgdh*. Hence, this methodology will be useful for cDNA rescue experiments that require the correct expression pattern of tested genes.

Cloning and Transgenesis

A pCaSpeR4 vector having ~5kb genomic DNA fragment that contains promoter (1003bp), coding sequences (3633 bp), and 3'UTR (456 bp) of *dNrd1* were generously provided by A. Leibfried and A. Ephrussi (not published). The insert is cloned into BamHI and NotI sites in pCaSpeR4. We subcloned *dNrd1* genomic fragment into BglII and NotI sites in pattB vector (Bischof et al., 2007) (*pattB-gRes-dNrd1-WT*). The construct was injected into *y,w,ΦC31; VK5* (Venken et al., 2006) embryos, and the transgenic flies were selected.

RE02581, an EST of *dNrd1*, (purchased from DGRC) contains two base pair changes that cause substitution of two amino acids (R13G and A801A). These mutations were corrected by site-directed PCR using primers: dNrd1-R13-F: 5'-acagCGCACATTTGTTTAGAcgaTTCGAATTTCACGTACGTAC, dNrd1-R13-R: GTACGTACGTGAAATTCGAATCGTCTAAACAAATGTGCGCTGT-3', dNrd1-A801-F: 5'-GCAACTATACGGAAGAGTCCgctCATAATGTAATGAACTCGTTG-3', dNrd1-A801-R: 5'-CAACGAGTTCATTACATTATGAGCGGACTCTTCCGTATAGTTGC-3'. The corrected dNrd1 EST clone was amplified by PCR and used for construction of pUASTattB-dNrd1-V5 and pUASTattB-ΔMTS dNrd1-V5. The PCR reactions were performed by using following primers: dNrd1-F EcoRI: 5'-tttgGAATTCCAAAATGCTCTGGCAGCGATACAG-3', dNrd1 Δ1-42aa-F EcoRI: 5'-tttgGAATTCCAAAATGACCGACCAGGTCAAGTATC-3' and dNrd1-V5-R NotI: 5'-ctaaGCGGCCGCTTAGGTGCTATCCAGTCCGAGCAGTGGATTCGGGATCGGCTTGCC*GCCGCTTCC*CACC TGGCGGATTGCATCCGC-3'. For generating pUASTattB-dNrd1 [E161A], we performed site-directed

mutagenesis using the primers: 5'- CAGGGACTGGCACACTTTCTCgCgCACATGATCTTTATGGGCTC -3' and 5'- GAGCCCATAAAGATCATGTGCGCGAGAAAGTGTGCCAGTCCCTG-3'.

For construction of pUASTattB-human NRD1-V5, -human NRD1 (p.M636VfsX2)-V5, and -human ΔMTS NRD1-V5, a full-length NRD1 cDNA, a NRD1 cDNA carrying M636VfsX2 variant from the patient (Figure 2A-B) or a NRD1 cDNA that lacks nucleotides corresponding to the MTS was amplified by PCR from a human NRD1 cDNA clone **(**3138712, Invitrogen**),** and then subcloned into pUASTattB vector (Bischof et al., 2007) using primers: NRD1-F NotI: 5'-tttgGCGGCCGCCAAAATGCTGAGGA GAGTCACTGTTG-3', NRD1-V5-R XhoI: 5'-ctaaCTCGAGTTAGGTGCTATCCAGTCCGAGCAGTGGATTCGGGATCGGCTTGCCGCCGCTTCCTTTGAC TATTTTATGGTAGG-3', NRD1 M636VfsX2-V5-R XhoI: 5'- cctaaCTCGAG TTAGGTGCTATCCAGTCCGAGCAGTGGATTCGGGATCGGCTTGCC GCCGCTTCC cacGTTTTCCACATACTCAACTGG -3', and NRD1 Δ1-49aa-F NotI: 5'-tttgGCGGCCGCCAAAATGCCTGGAAGGAACAAGGC-3'. For construction of pUASTattB-dOgdh-Flag, a coding sequence was amplified by PCR from the cDNA clone (RE42354, DGRC) and subcloned into pUASTattB vector using primers: dOgdh-PF_F BclI: 5'-attttgTGATCACAAA ATGCATAGAGCCCACACAGCC-3' and dOgdh-PF-Flag_R XbaI: 5'-agtaaTCTAGATTACTTGTCGTCATCGTCCTTGTAATC GCCGCTTCC GGTCGAAATCGCGTCGTTGAG-3'.

For constructing, pUASTattB- OGDHL, pUASTattB-OGDHL-Flag, pUAST-OGDH, and pUASTattB- OGDH-Flag, the following primers were used for amplifying coding sequences from cDNA clones of OGDH (MHS6278-202806532, GE Healthcare) and (MHS6278-202828499, GE Healthcare): hOGDHL-F NotI: 5'-attttGCGGCCGCAAA ATGAGTCAGCTGAGGCTGCTG-3', hOGDHL R XhoI: 5'-agtaaCTCGAGCTAAAATGTCTTGCCCTCAAAGGC-3', hOGDHL-Flag R XhoI: 5'-agtaaCTCGAG TTACTTGTCGTCATCGTCCTTGTAATCAATATCGTGGTCCTTGTAGTC GCCGCTTCC AAATGTCTTGCCCTCAAAGGC-3', hOGDH -F NotI: 5'-attttGCGGCCGCAAA ATGTTTCATTTAAGGACTTGT-3', hOGDH-R XhoI: 5'-agtaa CTCGAGCTACGAGAAGTTCTTGAAGACGTC-3', hOGDHL-Flag R XhoI: 5'-agtaa CTCGAG TTACTTGTCGTCATCGTCCTTGTAATCAATATCGTGGTCCTTGTAGTC GCCGCTTCC CGAGAAGTTCTTGAAGACGTC-3'

pUASTattB-dOgdh (S793L)-Flag, pUASTattB-hOGDHL (S778L), pUASTattB-hOGDHL (S778L)-Flag, pUASTattB-hOGDH (S791L) and pUASTattB-hOGDH (S791L)-Flag were generated by site-directed mutagenesis PCR using primers: dOgdh_S793L-F: 5'-GAAGGCATGGGCCCCGAGCACTtgTCGTGCCGCGTGGAGCGCTTC-3',

dOgdh_S793L-R: 5'-GAAGCGCTCCACGCGGCACGAcaAGTGCTCGGGGCCCATGCCTTC-3', OGDHL_S778L-F: 5'-GAAGGCATGGGCCCAGAGCACTtGTCAGCGAGGCCCGAAAGGTTC-3', OGDHL_S778L-R: 5'-GAACCTTTCGGGCCTCGCTGACaAGTGCTCTGGGCCCATGCCTTC-3', OGDH_S791L-F: 5'-GAGGGCATGGGTCCAGAACATTtgTCCGCCCGCCCAGAGCGGTTC-3', OGDH_S791L-R: 5'-GAACCGCTCTGGGCGGGCGGAcaAATGTTCTGGACCCATGCCCTC-3'

A series of *pUASTattB-dNrd1* and *human NRD1* constructs were injected into *y,w,ΦC31; VK33* embryos. A series of *pUASTattB-dOgdh*, *OGHDL* and *OGDH* constructs were injected into *y,w,ΦC31; VK37* embryos, and transgenic flies were selected.

For constructing pUASTattB-l(2)tid-Myc, pUASTattB-Hsp60C-Myc, and pUASTattB-Hsc70-5-Myc, the following primers were used for amplifying coding sequences from EST clones (SD10289, AT13565, GM13788, DGRC): l(2)tid-PA_F EcoRI: 5'-attttGAATTCAAA ATGATGATTTCGTGTAAAAAATTA-3', l(2)tid-PA Myc_R NotI: 5'-gtaaGCGGCCGC TTACAGATCCTCTTCTGAGATGAGTTTCTGCTCgccgcttcc CTCGCTCGTTGCTTGCTTACT-3', Hsp60C-PA_F EcoRI: 5'-attttGAATTCAAA ATGATGCGCATGTTCCGTTAC-3', Hsp60C-PA Myc_R NotI: 5'-gtaaGCGGCCGC TTACAGATCCTCTTCTGAGATGAGTTTCTGCTCgccgcttcc CATGCCCATTCCGCCCATG-3', Hsc70-5-PA_F NotI : 5'-ttttGCGGCCGCAAA ATGCTGCGCGTACCCAAGTTTC-3', Hsc70-5-PA Myc_R XhoI: tgtaa 5'-CTCGAG TTACAGATCCTCTTCTGAGATGAGTTTCTGCTCgccgcttcc GTTCTTCTCTTCCTTCTTGGC-3'

The DNA template for *in vitro* transcription was generated by PCR from pUASTattB-dOgdh-Flag construct using a pair of primers: 5'-aacaagaaac TAATACGACTCACTATAGGG-3' and 5'-aaatttCCACCATGCATAGAGCCCACACAGCC and ttttttttttttttttttttttttttttt TTACTTGTCGTCATCGTCCTTGTA-3'.

For constructing psiCheck-2-DOGDH-Rluc, the full length dOgdh cDNA with 4x(GSG)-SLAT linker was cloned into NheI site in front of Renilla luciferase coding sequence in frame. The following primers were used for amplifying coding sequence of dOgdh from pUASTattB-dOgdh construct:

dOGDH F-XbaI: 5'-atggcTCTAGA gccacc ATGCATAGAGCCCACACAG-3', dOGDH R_linker-XbaI: 5'-agcagTCTAGAct GCCGCTTCC GCCGCTTCC GCCGCTTCC GCCGCTTCCGGTCGAAATCGCGTCGTTGAG-3'

The direction of cloned dOgdh-4x(GSG)-SLAT linker in psiCheck-2-DOGDH-Rluc was confirmed by sequencing.

DNRD1 Antibody Production

N-terminal 627 bp DNA fragment of *dNrd1* was amplified using primers: 5'-tcatGAATTCATGACCGACCAGGTCAAGTATC-3' and 5'-cgtaGCGGCCGCcACGCCTGGTCTCATCATCCTG-3'. PCR product was digested with EcoRI and NotI, and cloned into pET28a vector. The clone was transformed into BL21 competent cells. The transformed cells were grown at 20°C overnight, and induced to express protein by adding 1mM IPTG. After 3 hours induction, cells were harvested. Protein was extracted using BugBuster reagent (Novagen, Cat. 70921-4) and purified using Ni-NTA (Qiagen). Purified protein was sent to Cocalico Biologicals (Reamstown, PA), and injected into guinea pigs to produce antibody.

Electroretinograms

ERG recording was carried out as previously described (Sandoval et al., 2014). Briefly, adult flies were glued to a glass slide. A recording probe was placed on the surface of the eye, and a reference probe was inserted into the thorax. A fly eye was exposed to a flash of white light for 1 sec. Responses were recorded and analyzed with AXON^{TM}-pCLAMP8 software.

Bright Field Imaging

Fly heads were dissected and fixed in 4% paraformaldehyde, 2% glutaraldehyde, 0.1M sodium cacodylate, and 0.005% $CaCl_2$ (pH7.2) at 4°C overnight. The heads were post-fixed with OsO_4, dehydrated in ethanol and propylene oxide, and then embedded in Embed-812 resin (Electron Microscopy Sciences). One micron-thick sections of PRs were stained with toluidine blue and imaged with a Zeiss microscope (Axio Imager-Z2) equipped with an AxioCam MRm digital camera. Images were processed with Adobe Photoshop.

Dissection and Immunostaining

For muscle and axon staining, dissection of third instar larvae was performed as descried in the book chapter: The neuromuscular junction in *Drosophila* protocols (Bellen and Budnik, 2000). Briefly, third instar larvae were fixed in 4% formaldehyde for 30 min at room temperature and washed in PBS containing 0.3% Triton X-100. The primary antibodies were used at the following dilutions: mouse anti-ATP5A 1:500 (Abcam Cat# ab14748 RRID:AB_301447), chick anti-GFP 1:1000 (Abcam Cat# ab13970 RRID:AB_300798), rabbit anti-GFP 1:1000 (Molecular Probes Cat# A-11122 RRID:AB_221569), rabbit Gdh 1: 200 (Abcam Cat# ab34786 RRID:AB_732619), mouse anti-V5 1: 500 (Thermo Fisher Scientific Cat# R960-25 RRID:AB_2556564), rabbit anti-HRP 1:1000

(Jackson ImmunoResearch Cat# 123-495-021). Alexa 488 conjugated (Thermo Fisher Scientific Cat# A-11034 RRID:AB_2576217), and Cy3 conjugated secondary antibodies (Jackson ImmunoResearch Labs Cat# 715-165-150 RRID:AB_2340813) were used at 1:200. Samples were mounted in Vectashield (Vector Labs, Burlingame, CA). Imaging was performed using LSM510 confocal microscope (Zeiss). Images were processed with Zeiss LSM Image Browser and Adobe Photoshop.

Quantitative PCR for mtDNA Content

Method is adapted from (Bai and Wong, 2004). *Drosophila* whole DNA (genomic and mitochondrial) was purified from third instar larvae as the template for PCR. The template DNA was mixed with primers and green supermix reagent (iQ SYBR; Bio-Rad Laboratories). PCR was performed in a thermal cycler (iCycler; Bio-Rad Laboratories), and the data were collected and analyzed using the optical module (iQ5; Bio-Rad Laboratories) and related software following the manufacturer's instructions. The following primer pairs were used to amplify a genomic DNA fragment corresponding to CG9277/β-Tubulin or a mitochondrial DNA fragment corresponding to CG34083/ND5, respectively: β-Tubulin forward, 5′-CCTTCCCACGTCTTCACTTC-3′; and β-Tubulin reverse, 5′-TTCTTGGCATCGAACATCTG-3′; and ND5 forward, 5′-GCAGAAACAGGTGTAGGAGCA-3′; and ND5 reverse, 5′-GCTGCTATAACTAAAAGAGCTCAGA-3′. Dissociation curves for the amplicons were generated after each run to confirm that the fluorescent signals were not attributable to nonspecific signals (primer-dimers). The mtDNA content (mtDNA/ β-Tubulin ratio) was calculated using the formula: mtDNA content $=1/2^{\Delta Ct}$, where $\Delta Ct=Ct^{mtDNA\Delta}-Ct^{\beta\text{-Tubulin}}$.

Mitochondrial Functional Assay

Measuring mitochondrial membrane potential by tetramethylrhodamine ethyl ester (TMRE; Molecular Probes, Life Technologies) was carried out in live larval muscle as previously described (Shidara and Hollenbeck, 2010). Live images were taken using a 40x water immersion lens and a Zeiss LSM510 confocal microscope. NADH and ATP levels were measured from whole larval lysates using NAD/NADH Assay kit (abcam, ab65348) and ATP determination kit (A22066, Life Technologies). The ETC enzymatic activity assay was carried out as previously described (Graham et al., 2010). The enzyme activity of OGDH, IDH, MDH, and Aconitase was determined from isolated mitochondria using kits (K678-100, BioVision; K756-100, BioVision; K654-100, BioVision; K716-100, BioVision). Mitochondria were isolated as previously described (Graham et al., 2010). Briefly, an100 µl volume of larvae was homogenized in mitochondrial isolation buffer (225 mM mannitol, 75mM sucrose, 5 mM Hepes [pH7.4], 1 mM EGTA, 0.5% bovine serum albumin (BSA)) using a Dounce homogenizer on ice. Tissue lysates were centrifuged at 1,500*g* for 5 min at 4°C. Supernatants were transferred to fresh tube, and centrifuged at 8,000*g* for 15 min to precipitate mitochondria. Discard soup and spare mitochondria pellets for further assays.

Cell Culture

S2 cells were grown in Schneider's *Drosophila* medium (Life Technologies) supplemented with 10% fetal bovine serum (FBS) and Penicillin-Streptomycin (Sigma) at room temperature (21°C). Mouse embryonic fibroblasts (MEFs) were grown in DMEM (10569-010, Life Technologies) supplemented with 5% FBS and Penicillin-Streptomycin and grown at 37°C.

Western Blot

Fly larvae or heads were homogenized in 1x Laemmli sample buffer containing 2.5% β-mercaptoethanol (Sigma-Aldrich). After boiling for 5 min, samples were loaded into 4-20% Mini-PROTEAN® TGX gel (Bio-Rad), separated by SDS-PAGE, and transferred to nitrocellulose membranes (Bio-Rad). The following antibodies were used: mouse anti-PDH-1α (MitoScience LLC Cat# MSP07 RRID:AB_478296), 1:1,000; mouse anti-NDUFS3

(MitoScience LLC Cat# MS112 RRID:AB_478239), 1:1,000; mouse anti-ATP5A (Abcam Cat# ab14748 RRID:AB_301447), 1:1,000; chicken anti-Porin (Graham et al., 2010), 1:3,000; mouse anti-Cyt C (MitoScience LLC Cat# MSA06 RRID:AB_478285), 1:1,000; mouse anti-actin C4 (MP Biomedicals Cat# 08691002 RRID:AB_2335304), 1:2,000; rabbit anti-p62 (Rui et al., 2015), 1:3,000; rabbit anti- phospho-p70 S6 kinase (Thr398) (Cell Signaling Technology Cat# 9209S RRID:AB_2269804), 1:1,000; rabbit anti-S6 kinase (Santa Cruz Biotechnology Cat# sc-9027 RRID:AB_2182106), 1:1,000; rabbit anti-S6 kinase (Cell Signaling Technology Cat# 9202 RRID:AB_331676), 1:1,000; rabbit anti-phospho-4E-BP1 (Thr37/46) antibody (Cell Signaling Technology Cat# 2855 RRID:AB_560835), 1: 1,000; rabbit anti-4E-BP1 (Cell Signaling Technology Cat# 9452S RRID:AB_10693791), 1: 1,000; rabbit anti-LC3B (Cell Signaling Technology Cat# 2775 RRID:AB_915950), 1:1,000.

Co-Immunoprecipitation

pUASTattB constructs containing cDNAs (e.g. pUASTattB-dNrd1-V5 and pUASTattB-DOGDH-Flag) were transfected into S2 cells together with pAct5-Gal4 (Arbouzova et al., 2006) using Effectene (Qiagen). After 2 days of transfection, cells were washed with ice-cold PBS and collected by centrifugation. Collected cells were lysed in a co-IP buffer (50 mM Tris pH7.4, 150 mM NaCl, 10% glycerol, 0.5% NP-40) containing cOmplete protease inhibitor (Roche). The cell lysates were vortexed every 5 min and placed on ice for 30min, and then centrifuged at 20,000g for 15 min at 4°C. Supernatants were transferred into fresh tubes, and 5 % of supernatants were spared for inputs. The remainder was rotated with anti-V5 resin (A7345, Sigma) or anti-Myc resin (E6654, Sigma) overnight at 4°C. The resins were collected by spinning at 5,000g for 30 sec at 4°C. Supernatants were discarded. The resins were washed with the co-IP buffer three times at 4°C.

For *in vivo* co-IP, *DOGDH-GFP* larvae were homogenized with co-IP buffer containing cOmplete (Roche) using a Dounce homogenizer. Tissue debris was removed by centrifugation at 20,000g for 15 min at 4°C. Clear supernatants were rotated with 15µl of GFP-Trap resin or control resin (Chromotek) for 2 hours at 4°C. Resins were collected by brief spin, and washed with 1ml of co-IP buffer three times at 4°C. Resin-bound proteins were eluted by applying 50µl of elution buffer (Chromotek). The co-precipitated proteins were analyzed by western blot using anti-Flag M2 antibody (Sigma-Aldrich Cat# F1804 RRID:AB_262044), anti-V5 antibody (Thermo Fisher Scientific Cat# R960-25 RRID:AB_2556564), and anti-Myc (9B11) antibody (Cell Signaling Technology Cat# 2040 RRID:AB_2148465).

Mitochondrial Import Assay

For an import assay, C-terminally Flag-tagged DOGDH protein was produced from a DNA fragment that contains a T7 promoter, coding sequence of *Drosophila* OGDH followed by 2xFlag sequence and polyA using T_NT® T7 Quick coupled transcription/translation system (L1170, Promega). A total of 200 µg of isolated mitochondria was resuspended in 500 µl of mitochondria import assay buffer (MIAB) (250 mM MOPS/KOH, pH7.2, 2.5mM $MgCl_2$, 80 mM KCl, 3% BSA, 2 mM NADH) and pre-incubated at 27°C for 2-3 min. Subsequently, the pre-incubated mitochondria were mixed with DOGDH-Flag protein, and incubated. The reaction was stopped at multiple time points by adding ice-cold SEM buffer (250 mM sucrose, 1 mM EDTA, 10 mM MOS/KOH, pH7.2) containing cOmplete protease inhibitor (Roche). Mitochondria were isolated and washed in SEM buffer three times by centrifugation at 8,000g for 10 min at 4°C. Imported DOGDH-Flag in mitochondria was analyzed by western blot with anti-Flag M2 antibody (Sigma-Aldrich Cat# F1804 RRID:AB_262044).

Mitochondrial Luciferase Aggregation Assay

To test mitochondrial chaperone activity of DNRD1, we developed the mitochondrial luciferase aggregation assay by modifying cytosolic luciferase aggregation assay (Ali et al., 2016; Michels et al., 1997). We constructed a *psiCheck-dOgdh-renilla luciferase* reporter (DOGDH-Rluc reporter) by cloning full length DOGDH coding sequence in front of renilla luciferase in frame. This reporter and pAct-Gal4 was transfected into S2 cells with or without *pUASTattB-dNrd1* using Effectene (Qiagen). After 72 hr transfection, the cells were treated with cycloheximide (50 µg/mL for 3 hrs). One batch of cells was lysed immediately with 1x passive lysis buffer

(Promega), which the other two batches were heat-shocked at 42°C for 15 min. The second batch of cells was lysed immediately after heat shock, while the last batch was incubated at 37°C for 3 hrs to recover DOGDH-Rluc reporter activity. Luciferase activity was measured with the Luciferase Assay system (Promega) and the TD-20/20 Luminometer (Turner Designs).

Mass Spectrometry Procedure for Identification of DNRD1-interacting Proteins

1ml volume of larvae expressing DNRD1-V5 (*da-Gal4>UAST-dNrd1-V5*) or control (*da-Gal4/+)* were homogenized in lysis buffer (50 mM Tris pH7.4, 150 mM NaCl, 10% glycerol, 0.5% NP-40) containing cOmplete protease inhibitor (Roche) and phosphatase inhibitor (P3200, GenDEPOT) using Dounce homogenizer. Homogenized samples were subjected to centrifugation at 20,000g for 15 min at 4°C. Supernatants were centrifuged at 100,000g for 30 min at 4°C. Supernatants (20mg/ml) were incubated with 5 µg of anti-V5 antibody (R960, life technologies) in a rotator at 4°C. Purified DNRD1 complex was resolved on SDS-PAGE (4–20% Tris/glycine gel [Novex; Invitrogen]). Coomassie brilliant blue–stained protein bands were excised and subjected to in-gel digestion with trypsin essentially as previously described (Jung et al., 2005). Vacuum dried peptide was dissolved in 10 µl of loading solution (5% methanol containing 0.1% formic acid) and half of reconstituted samples were subjected to nanoLC-MS/MS analysis with a nano-LC II (Thermo Scientific) coupled to Thermo Velos pro (Thermo Scientific) mass spectrometer. The peptides were loaded onto an in-housed Reprosil-Pur Basic C18 (3 µm, Dr.Maisch GmbH, Germany) trap column which was 2 cm X 75 µm size. Then the trap column was washed with loading solution and switched in-line with an in-housed 10 cm x 75 µm column packed with Reprosil-Pur Basic C18 equilibrated in 0.1% formic acid/water. The peptides were separated with a 45 min discontinuous gradient of 5-28% acetonitrile/0.1% formic acid at a flow rate of 800 nl/min. Separated peptides were directly electro-sprayed into mass spectrometer. The instrument was operated in the data-dependent mode acquiring fragmentation spectra of the top 35 strongest ions and under direct control of Xcalibur software (Thermo Scientific). Parent MS spectrum and CID fragmented MS/MS spectrum were acquired in the Orbitrap with resolution of 70,000 and 17,500. The full MS range was 375-1300 m/z and the trap target was 3,000,000. MS/MS ion target value was 100,000 ions and the ion selection threshold was 13,000 count. Obtained MS/MS spectra were searched against target-decoy Mouse refseq database in Proteome Discoverer 1.3 interface (PD1.3, Thermo Fisher) with Mascot algorithm (Mascot 2.3, Matrix Science) using Flybase protein database. The precursor mass tolerance was confined within 20 ppm with fragment mass tolerance of 0.5 Dalton and a maximum of two missed cleavage was allowed.

Fly Genetics and Rapamycin feeding

To overexpress Atg1, we crossed *P{GMR-hid}SS1, y1w*P{neoFRT}19A/y; ey-Gal4, UAS-FLP (II) males with* $dNrd1^{B}$*/FM7, Kr-Gal4, UAS-GFP; UAS-Atg1* females. These crosses were placed at 18°C until eclosion of adult flies. The eclosed adult flies transferred to new vials and were incubated in a daily light/dark cycle (at 25°C for 12 hrs with light and at 21°C for 12 hrs with dark) for 35 to 38 days before ERG assay. To overexpressed dominant negative S6k, (*UAS-S6k.KO*), we crossed *P{GMR-hid}SS1, y1w*P{neoFRT}19A/Y; Rh1-Gal4, UAS-FLP (II) males with* $dNrd1^{A}$*/FM7, Kr-Gal4, UAS-GFP; UAS-S6k.KQ (*(Barcelo and Stewart, 2002) females and ERG assay was conducted 35-day-old progenies. Rapamycin (3µM) was fed every 3 days for flies whose PRs having *dNrd1* mutant clones or expressing *dOgdh* RNAi.

Metabolic Measurements Using Mass Spectrometry

Reagents and internal standards

High-performance liquid chromatography (HPLC) grade acetonitrile, methanol and water were purchased from Burdick & Jackson (Morristown, NJ). Mass spectrometry grade formic acid and internal standards namely, [15N]2Tryptophan-, Glutamic acid-d5, Thymine-d4, Gibberellic acid, Trans-Zeatin, Jasmonic acid, [15N] Anthranilic acid, and Testosterone-d3 were purchased from Sigma- Aldrich (St. Louis, MO). The calibration solution containing multiple calibrants in acetonitrile/trifluroacetic acid /water was purchased from (Agilent

Technologies, Santa Clara, CA).

Sample preparation for mass spectrometric analysis The metabolome extraction method described earlier was used for the cell lines and pooled liver controls in this study. Briefly, cells or fly extracts were thawed at 4°C and subjected to freeze-thaw cycle in liquid nitrogen and over the ice three times to rupture the cell membrane. Following this, an 750 µL of ice cold methanol: water (4:1) containing 20 µL of spiked internal standards (8) was added to each cell line. The cells were homogenized for 1 min (30 sec pulse twice) and mixed with 450 µl of ice cold chloroform and vortex mixed in a Multi-Tube Vortexer for 10 min. The resulting homogenate was mixed with 150 µl of ice cold water and vortexed again for 2 min. The homogenate was incubated at -20°C for 20 min and centrifuged at 4°C for 10 min to partition the aqueous and organic layers. The aqueous and organic layers were separated and dried at 37°C for 45 min in an Automatic Environmental Speed Vac® system (Thermo Fisher Scientific, Rockford, IL). The aqueous extract was reconstituted in 500 µl of ice cold methanol:water (50:50) and filtered through 3 KDa molecular filter (Amicon Ultracel -3K Membrane, Millipore Corporation, Billerica, MA) at 4°C for 90 min to remove proteins. The filtrate was dried at 37°C for 45 min in speed vac and stored at -80°C until mass spectrometry analysis. Prior to mass spectrometry analysis, the dried extract was resuspended in 100 µL of methanol:water (50:50) containing 0.1% formic acid and analyzed using Single Reaction Monitoring (SRM).

The tissues were stored at −140°C in liquid nitrogen until analysis. For extraction of the metabolome, 25 mg of tissue was homogenized in 1:4 ice-cold water:methanol mixture containing an equimolar mixture of 8 internal standard compounds. This was followed by metabolic extraction using sequential application of ice-cold organic and aqueous solvents (water:methanol:chloroform:water; ratio 1:4:3:1), deproteinization and drying of the extract as mentioned above.

Liquid Chromatography- Mass spectrometry: HPLC analysis was performed using an Agilent 1290 series HPLC system equipped with a degasser, binary pump, thermostatted autosampler and column oven (all from Agilent Technologies, Santa Clara, CA). The SRM-based measurement of relative metabolite levels, used either reverse phase or normal phase chromatographic separation**.** All samples were kept at 4°C and 5 µl was used for analysis.

Separation of TCA metabolites

Targeting the metabolites, the normal phase chromatographic separation was also used for targeted identification of metabolites. This employed solvents containing water (solvent A), with solvent A modified by the addition of 5mM Ammonium acetate (pH 9.9), and 100% acetonitrile (ACN) solvent B. The binary pump flow rate was 0.2 ml/min with a gradient spanning 80 % B to 2 % B over a 20 minute period followed by 2% B to 80% B for a 5 min period and followed by 80% B for 13 minute time period. The flow rate was gradually increased during the separation from 0.2 mL/min (0-20 mins), 0.3 mL/min (20.1-25 min), 0.35 mL/min (25-30 min), 0.4 mL/min (30-37.99 min) and finally set at 0.2 mL/min (5 min). Metabolites were separated on a Luna Amino (NH2) column (4µm, 100A 2.1x150mm, Phenominex), that was maintained in a temperature controlled chamber (37°C). All the columns used in this study were washed and reconditioned after every 50 injections.

Separation of amino acid metabolites

Targeted profiling (SRM) for the Amino acids, the RP chromatographic method employed a gradient containing water (solvent A) and acetonitrile (ACN, solvent B, with both solvents containing 0.2% Acetic acid and 0.1% formic acid). Separation of metabolites was performed on a Zorbax Eclipse XDB-C18 column (50 × 4.6 mm i.d.; 1.8 µm, Agilent Technologies, CA) maintained at 37°C. The binary pump flow rate was 0.2 ml/min with a gradient spanning 2% B to 95% B over a 25 minute time period.

The mass spectrometric analysis was performed on 6430 QQQ-LC/MS (Agilent Technologies, Santa Clara, CA). The mass spectrometer was operated in both electrospray positive and negative ionization modes, with a capillary voltage of either 3500 V (positive ionization) or 3000 V (negative ionization), a collision gas flow rate of 10 L/min and a nebulizer gas flow rate of 35 L/min. The temperature of nebulizer gas was maintained at 350°C. Nitrogen was used as the collision gas at a collision cell pressure of $2.39X10^{-5}$ Torr. For maximum sensitivity, the fragmentor voltage and collision energy for each metabolite were optimized separately using the optimizer® software (Agilent Technologies, Santa Clara, CA) and the optimized values were used for the SRM assays.

Whole-Exome Capture, Sequencing and Data analysis

All of the subjects enrolled in the BHCMG underwent whole-exome sequencing using methods that have been previously described in detail (Lupski et al., 2013). Produced sequence reads were mapped and aligned to the

GRCh37 (hg19) human genome reference assembly using the HGSC Mercury analysis pipeline (http://www.tinyurl.com/HGSC-Mercury/) (Reid et al., 2014). Variants were determined and called using the Atlas2 (Danecek et al., 2011) suite to produce a variant call file (VCF) (Bainbridge et al., 2011). High-quality variants were annotated using an in-house developed suite of annotation tools (Untergasser et al., 2012).

During the analyses of candidate variants/mutations observed after computational filtering, we further prioritized genes/variants using external publicly available databases. These included the 1000 Genomes Project (http://www.1000genomes.org) and other large-scale exome sequencing projects including the Exome variant server, NHLBI GO Exome Sequencing Project (ESP), Seattle, WA (http://evs.gs.washington.edu/EVS/), our "in-house-generated" exomes (from ~5,000 individuals participating in the BHCMG initiative) at Baylor College of Medicine (BCM) Human Genome Sequencing Center, and the Atherosclerosis Risk in Communities Study (ARIC) Database (http://drupal.cscc.unc.edu/aric/) (Gambin et al., 2015). The Exome Aggregation Consortium (ExAC), Cambridge, MA (URL: http://exac.broadinstitute.org) [Aug 2015] was used to search for homozygous loss-of-function variants in specific candidate genes.

Supplemental References

Ali, Y.O., Allen, H.M., Yu, L., Li-Kroeger, D., Bakhshizadehmahmoudi, D., Hatcher, A., McCabe, C., Xu, J., Bjorklund, N., Taglialatela, G., et al. (2016). NMNAT2:HSP90 Complex Mediates Proteostasis in Proteinopathies. PLoS Biol. *14*, e1002472.

Arbouzova, N.I., Bach, E.A., and Zeidler, M.P. (2006). Ken & barbie selectively regulates the expression of a subset of Jak/STAT pathway target genes. Curr. Biol. *16*, 80–88.

Bai, R.K., and Wong, L.J.C. (2004). Detection and quantification of heteroplasmic mutant mitochondrial DNA by real-time amplification refractory mutation system quantitative PCR analysis: A single-step approach. Clin. Chem. *50*, 996–1001.

Bainbridge, M.N., Wang, M., Wu, Y., Newsham, I., Muzny, D.M., Jefferies, J.L., Albert, T.J., Burgess, D.L., and Gibbs, R.A. (2011). Targeted enrichment beyond the consensus coding DNA sequence exome reveals exons with higher variant densities. Genome Biol. *12*, R68.

Barcelo, H., and Stewart, M.J. (2002). Altering Drosophila S6 kinase activity is consistent with a role for S6 kinase in growth. Genesis *34*, 83–85.

Baxter, P.S., Rigby, a. S., Rotsaert, M.H.E.P.D., and Wright, I. (2009). Acquired Microcephaly: Causes, Patterns, Motor and IQ Effects, and Associated Growth Changes. Pediatrics *124*, 590–595.

Bellen, H.J., and Budnik, V. (2000). The neuromuscular junction. In Drosophila Protocols, M. Ashburner, and R.S. Hawley, eds. (New York: Cold Spring Harbor Laboratory Press), pp. 175–199.

Bischof, J., Maeda, R.K., Hediger, M., Karch, F., and Basler, K. (2007). An optimized transgenesis system for Drosophila using germ-line-specific phiC31 integrases. Proc. Natl. Acad. Sci. U. S. A. *104*, 3312–3317.

Danecek, P., Auton, A., Abecasis, G., Albers, C. a., Banks, E., DePristo, M. a., Handsaker, R.E., Lunter, G., Marth, G.T., Sherry, S.T., et al. (2011). The variant call format and VCFtools. Bioinformatics *27*, 2156–2158.

Diao, F., Ironfield, H., Luan, H., Diao, F., Shropshire, W.C., Ewer, J., Marr, E., Potter, C.J., Landgraf, M., and White, B.H. (2015). Plug-and-Play Genetic Access to Drosophila Cell Types using Exchangeable Exon Cassettes. Cell Rep. *10*, 1410–1421.

Gambin, T., Jhangiani, S.N., Below, J.E., Campbell, I.M., Wiszniewski, W., Muzny, D.M., Staples, J., Morrison, A.C., Bainbridge, M.N., Penney, S., et al. (2015). Secondary findings and carrier test frequencies in a large multiethnic sample. Genome Med. *7*, 54.

Gnerer, J.P., Venken, K.J.T., and Dierick, H.A. (2015). Gene-specific cell labeling using MiMIC transposons. Nucleic Acids Res. *43*, e56–e56.

Graham, B.H., Li, Z., Alesii, E.P., Versteken, P., Lee, C., Wang, J., and Craigen, W.J. (2010). Neurologic

dysfunction and male infertility in Drosophila porin mutants: A new model for mitochondrial dysfunction and disease. J. Biol. Chem. *285*, 11143–11153.

Jung, S.Y., Malovannaya, A., Wei, J., O'Malley, B.W., and Qin, J. (2005). Proteomic analysis of steady-state nuclear hormone receptor coactivator complexes. Mol. Endocrinol. *19*, 2451–2465.

Lupski, J.R., Gonzaga-Jauregui, C., Yang, Y., Bainbridge, M.N., Jhangiani, S., Buhay, C.J., Kovar, C.L., Wang, M., Hawes, A.C., Reid, J.G., et al. (2013). Exome sequencing resolves apparent incidental findings and reveals further complexity of SH3TC2 variant alleles causing Charcot-Marie-Tooth neuropathy. Genome Med. *5*, 57.

van Maldegem, B.T., Wanders, R.J. a., and Wijburg, F. a. (2010). Clinical aspects of short-chain acyl-CoA dehydrogenase deficiency. J. Inherit. Metab. Dis. *33*, 507–511.

Michels, A.A., Kanon, B., Konings, A.W., Ohtsuka, K., Bensaude, O., and Kampinga, H.H. (1997). Hsp70 and Hsp40 chaperone activities in the cytoplasm and the nucleus of mammalian cells. J. Biol. Chem. *272*, 33283–33289.

Reid, J.G., Carroll, A., Veeraraghavan, N., Dahdouli, M., Sundquist, A., English, A., Bainbridge, M., White, S., Salerno, W., Buhay, C., et al. (2014). Launching genomics into the cloud: deployment of Mercury, a next generation sequence analysis pipeline. BMC Bioinformatics *15*, 30.

Rui, Y.-N., Xu, Z., Patel, B., Chen, Z., Chen, D., Tito, A., David, G., Sun, Y., Stimming, E.F., Bellen, H.J., et al. (2015). Huntingtin functions as a scaffold for selective macroautophagy. Nat. Cell Biol. *17*, 262–275.

Shidara, Y., and Hollenbeck, P.J. (2010). Defects in mitochondrial axonal transport and membrane potential without increased reactive oxygen species production in a Drosophila model of Friedreich ataxia. J. Neurosci. *30*, 11369–11378.

Untergasser, A., Cutcutache, I., Koressaar, T., Ye, J., Faircloth, B.C., Remm, M., and Rozen, S.G. (2012). Primer3-new capabilities and interfaces. Nucleic Acids Res. *40*.

Venken, K.J.T., He, Y., Hoskins, R.A., and Bellen, H.J. (2006). P[acman]: a BAC transgenic platform for targeted insertion of large DNA fragments in D. melanogaster. Science *314*, 1747–1751.